NEOPLASIA
www.neoplasia.com

Volume 11 Number 5 May 2009 pp. 469–476 469

Truncation of the Catalytic Domain of the Cylindromatosis Tumor Suppressor Impairs Lung Maturation[1]

Eirini Trompouki*, Ageliki Tsagaratou*,†, Stylianos K. Kosmidis‡, Pascal Dollé§, Jun Qian¶, Dimitris L. Kontoyiannis*, Wellington V. Cardoso¶ and George Mosialos*,†

*Institute of Immunology, Biomedical Sciences Research Center Al. Fleming, 34 Al. Fleming Str, Vari 16672, Greece; †School of Biology, Aristotle University of Thessaloniki, 54124 Thessaloniki, Greece; ‡Institute of Molecular Biology and Genetics, Biomedical Sciences Research Center Al. Fleming, 34 Al. Fleming Str, Vari 16672, Greece; §Institut de Génétique et de Biologie Moléculaire et Cellulaire, INSERM, U964, CNRS, UMR 7104, Université de Strasbourg, 67404 Illkirch, France; ¶Pulmonary Center, Department of Medicine, Boston University School of Medicine, Boston, MA, 02118, USA

Abstract

Cyld encodes a 956–amino acid deubiquitinating enzyme (CYLD), which is a negative regulator of nuclear factor κB and mitogen-activated protein kinase pathways. Mutations that truncate and inactivate the carboxyl-terminal deubiquitinating domain of CYLD underlie the development of skin appendage tumors in humans, whereas down-regulation of *Cyld* expression has been associated with the development of various types of human malignancies including lung cancer. To establish an animal model of human CYLD inactivation and characterize the biological role of CYLD *in vivo*, we generated mice carrying a homozygous deletion of *Cyld* exon 9 ($Cyld^{\Delta 9/\Delta 9}$ mice) using a conditional approach. Deletion of exon 9 would cause a carboxyl-terminal truncation of CYLD and inactivation of its deubiquitinating activity. In accordance with previous studies, fibroblasts from $Cyld^{\Delta 9/\Delta 9}$ embryos had hyperactive nuclear factor κB and c-Jun kinase pathways compared with control fibroblasts. $Cyld^{\Delta 9/\Delta 9}$ newborn mice were smaller than wild-type littermates with a short and kinky tail and no major developmental defects. However, $Cyld^{\Delta 9/\Delta 9}$ mice died shortly after birth from apparent respiratory dysfunction. Histological examination of E18.5 $Cyld^{\Delta 9/\Delta 9}$ lungs demonstrated an immature phenotype characterized by hyperplasic mesenchyme but apparently normal epithelial, smooth muscle. and endothelial structures. Our study identifies an important role of CYLD in lung maturation, which may underlie the development of many cases of lung cancer.

Neoplasia (2009) 11, 469–476

Introduction

Hereditary mutations of the cylindromatosis tumor suppressor gene (*Cyld*) predispose humans to tumors of skin appendages known as cylindromas and trichoepitheliomas [1]. These tumors show characteristics of hair follicle differentiation and are usually benign, although rare cases of metastatic skin appendage tumors have been described [2]. Additional studies have associated *Cyld* down-regulation with the development of other types of human cancer including hepatocellular, colon, lung, and cervical cancers as well as multiple myeloma [3–9]. These findings highlight a broad tissue homeostatic activity of *Cyld*.

Abbreviations: JNK, c-Jun kinase; MEF, murine embryonic fibroblast; NF-κB, nuclear factor κB; NSCLC, non–small cell lung cancer; TNF, tumor necrosis factor; TRAF, TNF-receptor–associated factor

Address all correspondence to: George Mosialos, School of Biology, Aristotle University of Thessaloniki, 54124 Thessaloniki, Greece. E-mail: gmosialo@bio.auth.gr

[1]This work was supported by a Howard Hughes International Scholarship (G.M.) and by a grant from National Institutes of Health/National Heart, Lung, and Blood Institute (PO1 HL47049 to W.V.C. and J.Q.). G.M. is a Leukemia and Lymphoma Society Scholar.

Received 7 November 2008; Revised 24 February 2009; Accepted 25 February 2009

DOI 10.1593/neo.81424

Zhong et al. [4] have provided compelling evidence for an important role of *Cyld* in lung cancer development. *Cyld* was shown to be downregulated in nine non–small cell lung cancer (NSCLC) cell lines and in more than 60% of NSCLC cancer specimens tested. Importantly, exogenous expression of wild type but not catalytically inactive CYLD in NSCLC cell lines suppressed their growth. These findings identify a broad growth-suppressive role of CYLD in NSCLC development, which depends on its deubiquitinating activity.

Cyld codes for a 956–amino acid deubiquitinating enzyme (CYLD), which can inhibit activation of the transcription factor nuclear factor κB (NF-κB) by members of the tumor necrosis factor (TNF) receptor family (reviewed in Massoumi and Paus [10]). Notably, all the identified mutations of *Cyld* in human cylindromas are predicted to cause carboxyl-terminal truncations and inactivate the deubiquitinating domain of CYLD and its ability to inhibit NF-κB [1,11,12]. In addition to its effect on NF-κB, CYLD was shown to inhibit the activation of c-Jun kinase (JNK) and p38 in response to innate immunity stimuli [13,14]. The effects of CYLD on the NF-κB and mitogen-activated protein kinase pathways seem to be mediated at least in part through its ability to interact with TNF-receptor–associated factors 2 and 6 (TRAF2 and TRAF6), IκB kinase γ, transforming growth factor β–activated kinase 1, and Bcl3 (reviewed in Massoumi and Paus [10]).

Three groups reported the initial phenotypic characterization of mice with targeted inactivation of both *Cyld* alleles ($Cyld^{-/-}$ mice). Reiley et al. [15–17] identified a critical role for CYLD in thymocyte development and T and B lymphocyte activation. Massoumi et al. [18] reported an increased susceptibility of $Cyld^{-/-}$ mice to chemically induced skin tumors. This group went on to show that the development of skin tumors in $Cyld^{-/-}$ mice is associated with elevated cyclin D1 expression in $Cyld^{-/-}$ keratinocytes, which is NF-κB–dependent. Finally, Zhang et al. [19] reported increased colonic inflammation and colon cancer incidence in $Cyld^{-/-}$ mice compared with wild-type mice, after azoxymethane and dextran sulfate sodium administration. The three aforementioned teams inactivated *Cyld* by disrupting the translation-initiation-ATG–containing exon (exon 2). A fourth team reported recently the disruption of B-cell homeostasis in mice overexpressing solely an alternatively spliced CYLD product, which is catalytically active but lacks the TRAF2 and IκB kinase γ–interacting domains [20]. However, none of the targeting approaches mentioned mimic the identified mutations of *Cyld* in human tumors, which disrupt the catalytic domain of CYLD.

The present study used a conditional approach to introduce and characterize phenotypically a carboxyl-terminal truncating mutation of *Cyld* that mimics the characterized oncogenic human mutations. Our approach revealed a previously unidentified role of *Cyld* in lung

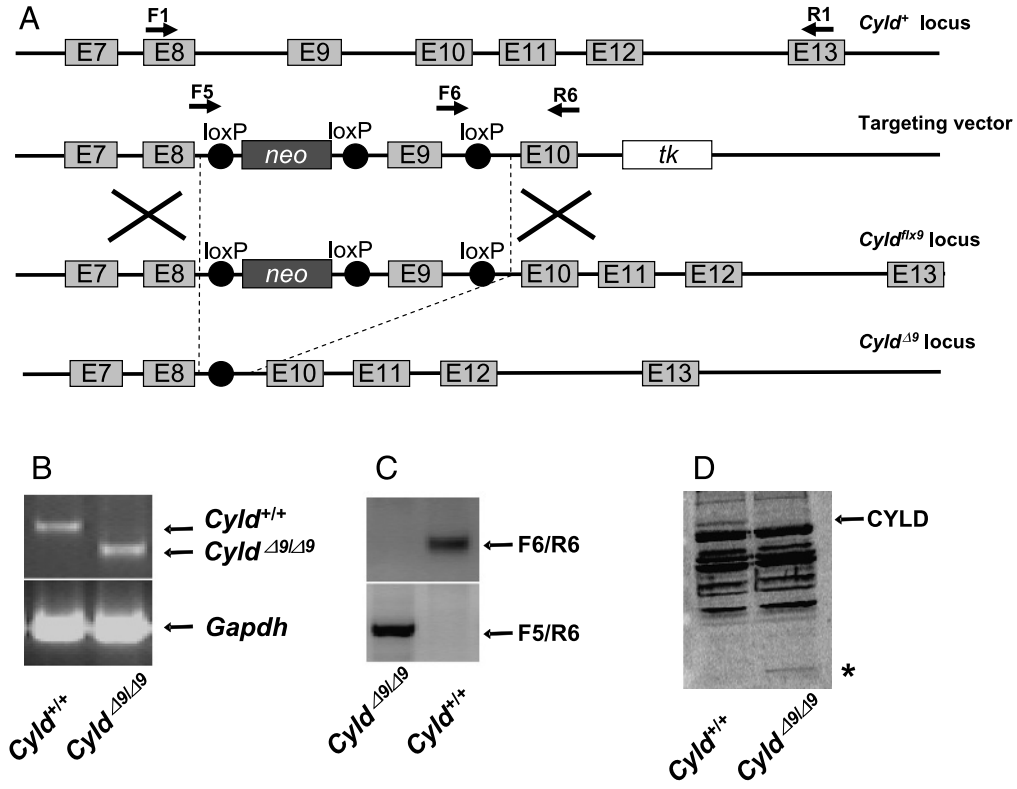

Figure 1. Generation of $Cyld^{\Delta 9/\Delta 9}$ mice. (A) The gene targeting strategy for inactivation of murine *Cyld*. Schematic representation of the exon/intron arrangement of the targeted *Cyld* locus on mouse chromosome 8, the targeting vector, and the conditional $Cyld^{flx9}$ locus before and after *Cre*-mediated recombination. The relative positions of loxP sites (filled circles), exons 7 (E7), 8 (E8), 9 (E9), 10 (E10), 11 (E11), 12 (E12), and 13 (E13), and primers used for RT-PCR (F1, R1) and genomic DNA PCR (F5, F6, R6) are also indicated. The positions of the neomycin resistance gene (*neo*) and the thymidine kinase gene (*tk*) in the targeting vector are shown by black and white rectangles, respectively. (B) RT-PCR of *Cyld* mRNA from fibroblasts isolated from $Cyld^{+/+}$ and $Cyld^{\Delta 9/\Delta 9}$ embryos using primers F1 and R1. *Gapdh* mRNA was used as a quantitative control. (C) PCR of genomic DNA isolated from tails of $Cyld^{+/+}$ and $Cyld^{\Delta 9/\Delta 9}$ mice using the indicated combinations of primers F5, F6, and R6. (D) Western blot analysis of lysates from fibroblasts isolated from $Cyld^{+/+}$ and $Cyld^{\Delta 9/\Delta 9}$ embryos using an anti-CYLD polyclonal antiserum. The positions of full-length CYLD (CYLD) and an amino-terminal polypeptide of CYLD (*) are shown.

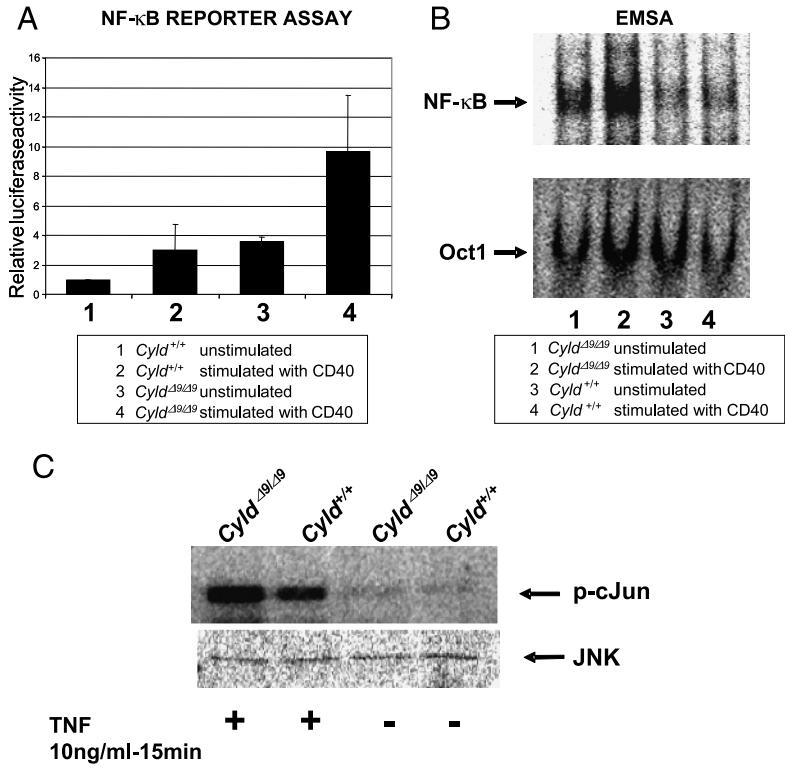

Figure 2. CYLD inactivation results in up-regulation of the NF-κB and JNK pathways. Fibroblasts from $Cyld^{+/+}$ and $Cyld^{\Delta 9/\Delta 9}$ embryos were used to evaluate the activities of NF-κB (A, B) and JNK (C). The basal and CD40 overexpression–induced activity of NF-κB was assessed by a luciferase reporter assay (A) and an electrophoretic mobility shift assay (EMSA, B). The DNA-binding activity of Oct-1 in the nuclear extracts used in (B) was used as a quantitative control. The basal and TNF-induced JNK activity was assessed by the ability of immunopurified JNK from the indicated embryonic fibroblasts (C, lower panel) to phosphorylate c-Jun *in vitro* (C, upper panel).

maturation and established a valuable mouse model for the delineation of the tissue-specific role of this tumor suppressor.

Materials and Methods

Targeted Mutation of the Murine Cyld *Gene*

The *Cyld* genomic locus was isolated from a 129Ola mouse genomic library. The targeting vector was designed to flank an exon 9–containing 0.95-kb *Hga*I-*Sal*I genomic fragment with loxP sites. The vector also consisted of a 4.95-kb *Bam*HI-*Hga*I genomic fragment as the 5′ arm of homology then a loxP-flanked neomycin resistance gene expression cassette, followed by a second 2.65-kb *Sal*I-*Cla*I genomic fragment as the 3′ arm of homology and a thymidine kinase expression cassette. The neomycin resistance gene was used for the positive selection of correctly targeted stem cells, and the thymidine kinase gene was used for the negative selection of incorrectly targeted embryonic stem cells. After identification by Southern blot (not shown), correctly targeted embryonic stem cell clones were injected onto C57/Bl6 blastocysts for chimera production and germ line transmission according to standard procedures [21]. Mice carrying the recombined $Cyld^{flx9}$ locus (Figure 1*A*) in the germ line were identified by genomic polymerase chain reaction (PCR) and crossed with *cre* transgenic mice expressing the Cre recombinase in the germ line [22]. Mice heterozygous for the deletion of *Cyld* exon 9 ($Cyld^{\Delta 9/+}$) were identified and crossed to generate homozygous mutant mice ($Cyld^{\Delta 9/\Delta 9}$). The following primers were used for reverse transcription–PCR (RT-PCR) or genomic PCR: F1: 5′-GCAGGCTGTACAGATGGAAC-3′, R1: 5′-CTCTGCAAATTTCAGGTTGCTGTTG-3′, F5: 5′-GCAGGCTGTACAGATGGAAC-3′, F6: 5′-CGTGAACAGATGTGATGAAGGC-3′, R6: 5′-CTACCATCCCTGCTAACCAC-3′. Experiments on live animals were approved by the Hellenic Ministry of Rural Development (Directorate of Veterinary Services) and by Biomedical Sciences Research Center Al. Fleming's Animal Research and Ethics Committee for compliance to FELASA regulations.

Measurement of NF-κB and JNK Activities

The basal and CD40 overexpression–induced activity of NF-κB in murine embryonic fibroblasts (MEFs) from $Cyld^{+/+}$ or $Cyld^{\Delta 9/\Delta 9}$ embryos was assessed by a luciferase reporter assay or an electrophoretic mobility shift assay as previously described [12]. The basal and TNF-induced JNK activity was assessed by the ability of immunopurified JNK from $Cyld^{+/+}$ or $Cyld^{\Delta 9/\Delta 9}$ MEF to phosphorylate c-Jun *in vitro* as previously described [23].

Immunohistochemistry and Immunoblot Analysis

Tissues were fixed in 4% paraformaldehyde in PBS overnight at 4°C and embedded in paraffin. For immunohistochemistry, tissue sections were deparaffinized and rehydrated. Endogenous peroxidase activity was quenched using 0.3% hydrogen peroxide in methanol. Sections were preincubated with the preimmune serum (rabbit or goat) and then with the primary antibody overnight at 4°C. The following antibodies were used: anti-human surfactant-associated protein C (SP-C; C-19; Santa Cruz Biotechnology Inc., Santa Cruz, CA), anti-Clara cell 10-kDa protein (CC10; goat, polyclonal anti-rabbit, gift from Drs Singh and Katyal, University of Pittsburgh), anti-Type 1 cell alpha

Table 1. Frequency of Genotypes of $Cyld^{+/+}$ $Cyld^{\Delta 9/+}$ and $Cyld^{\Delta 9/\Delta 9}$ Embryos and Newborns.

	$Cyld^{+/+}$	$Cyld^{\Delta 9/+}$	$Cyld^{\Delta 9/\Delta 9}$
E10.5 (n = 3)	5 (19%)	16 (62%)	5 (19%)
E12.5 (n = 2)	2 (15%)	7 (54%)	4 (31%)
E13.5 (n = 6)	9 (18%)	25 (50%)	16 (32%)
E14.5 (n = 3)	6 (26%)	13 (57%)	4 (17%)
E17.5 (n = 3)	6 (29%)	9 (43%)	6 (29%)
Newborns	9 (18%)	25 (51%)	15 (31%)*

Heterozygous $Cyld^{\Delta 9/+}$ mice were crossed and the genotype of newborns and embryos of the indicated embryonic stage were analyzed by genomic PCR. n indicates the number of litters analyzed.
*All $Cyld^{\Delta 9/\Delta 9}$ newborns died shortly after birth.

(T1 alpha mAB 8.1.1, Developmental Studies Hybridoma Bank, University of Iowa), anti-Sox2 (ab15830; Abcam), anti–smooth muscle actin (Sma; clone 1A4; Abcam, Cambridge, MA), and anti–platelet/endothelial cell adhesion molecule 1 (PECAM-1) (sc-71871; Santa Cruz Biotechnology) antibodies. Immunostaining was performed using the antirabbit and antigoat immunoglobulin G Vectastain and the DAB staining kits from Vector Laboratories (Burlingame, CA), according to the manufacturer's protocol. Sections were counterstained with methyl green. The expression of CYLD protein was determined by immunoblot analysis using a previously described anti-CYLD antiserum [15], which was a kind gift of Dr. Shao-Cong Sun (M.D. Anderson Cancer Center, TX).

Microtubule Depolymerization/Regrowth

Murine embryonic fibroblasts were treated with 5 μM nocodazole (Sigma, St. Louis, MO) for 30 minutes to depolymerize microtubules. Then the drug was washed out, and microtubules were allowed to regrow for 15 minutes. The cells were subsequently fixed with methanol and processed for immunofluorescence staining using an anti–α-tubulin antibody (catalog number T5168; Sigma).

In Vitro *Wound Healing/Cell Migration Assay*

Cell migration was assessed by the ability of the cells to migrate into a cell-free area. Cells were allowed to form a confluent monolayer in a six-well plate. The wound was made by scraping a conventional 20-μl pipette tip across the monolayer. Cell migration was monitored either after the cells were serum-starved overnight or after a 30-minute pretreatment of MEF with 5 μM nocodazole to induce microtubule depolymerization. Images of three different segments of the cell-free area were recorded at 0, 12, and 20 hours, and the distances traveled by the cells at the front in three different segments of the wound were measured.

Results

Generation of Mice with Targeted Mutation of Cyld

The purpose of our study was to assess the biological effects of catalytic inactivation of CYLD *in vivo* by generating an appropriate mouse model with mutated *Cyld* that mimics the identified oncogenic mutations of *Cyld* in human patients. Furthermore, a Cre-loxP–based conditional approach was used for *Cyld* inactivation to be able to study the biological role of *Cyld* in specific tissues. Exon 9 of murine *Cyld* was chosen for targeted deletion (Δ9) because it codes for an essential catalytic motif of the deubiquitination domain of CYLD and its removal places exon 10 and downstream exons out of frame after splicing

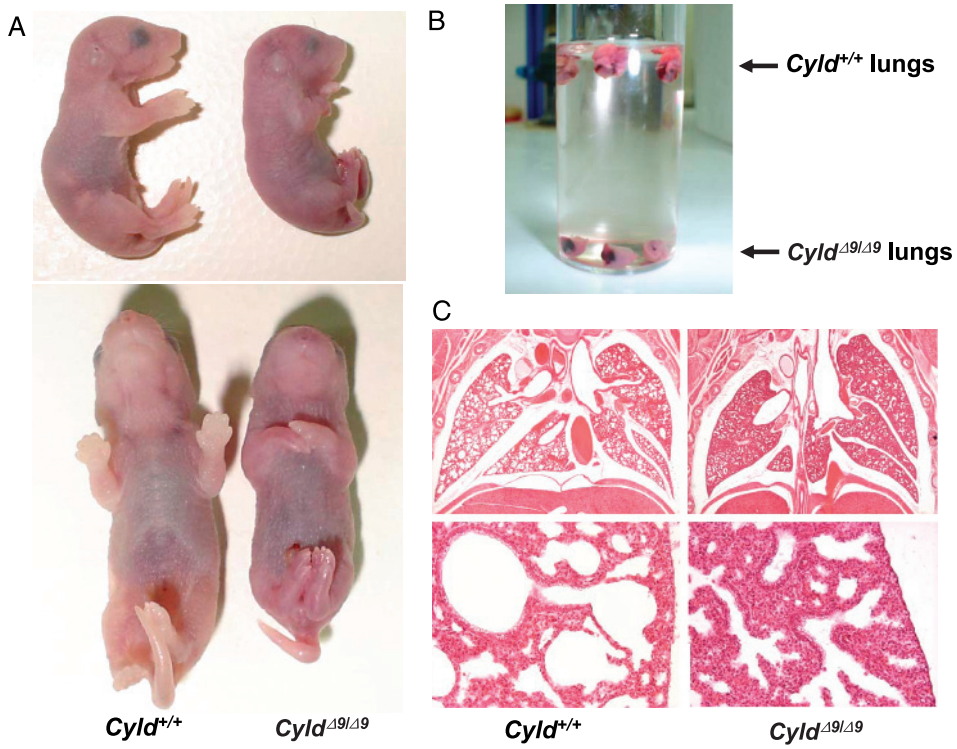

Figure 3. Phenotypic characteristics of lungs from wild-type and $Cyld^{\Delta 9/\Delta 9}$ mice and embryos. (A) Lateral (upper panels) and ventral (lower panels) views of wild-type and $Cyld^{\Delta 9/\Delta 9}$ mice at birth. (B) Buoyancy test of lungs from wild-type and $Cyld^{\Delta 9/\Delta 9}$ newborn mice. (C) Hematoxylin and eosin staining of lung tissue sections from E18.5 wild-type and $Cyld^{\Delta 9/\Delta 9}$ embryos.

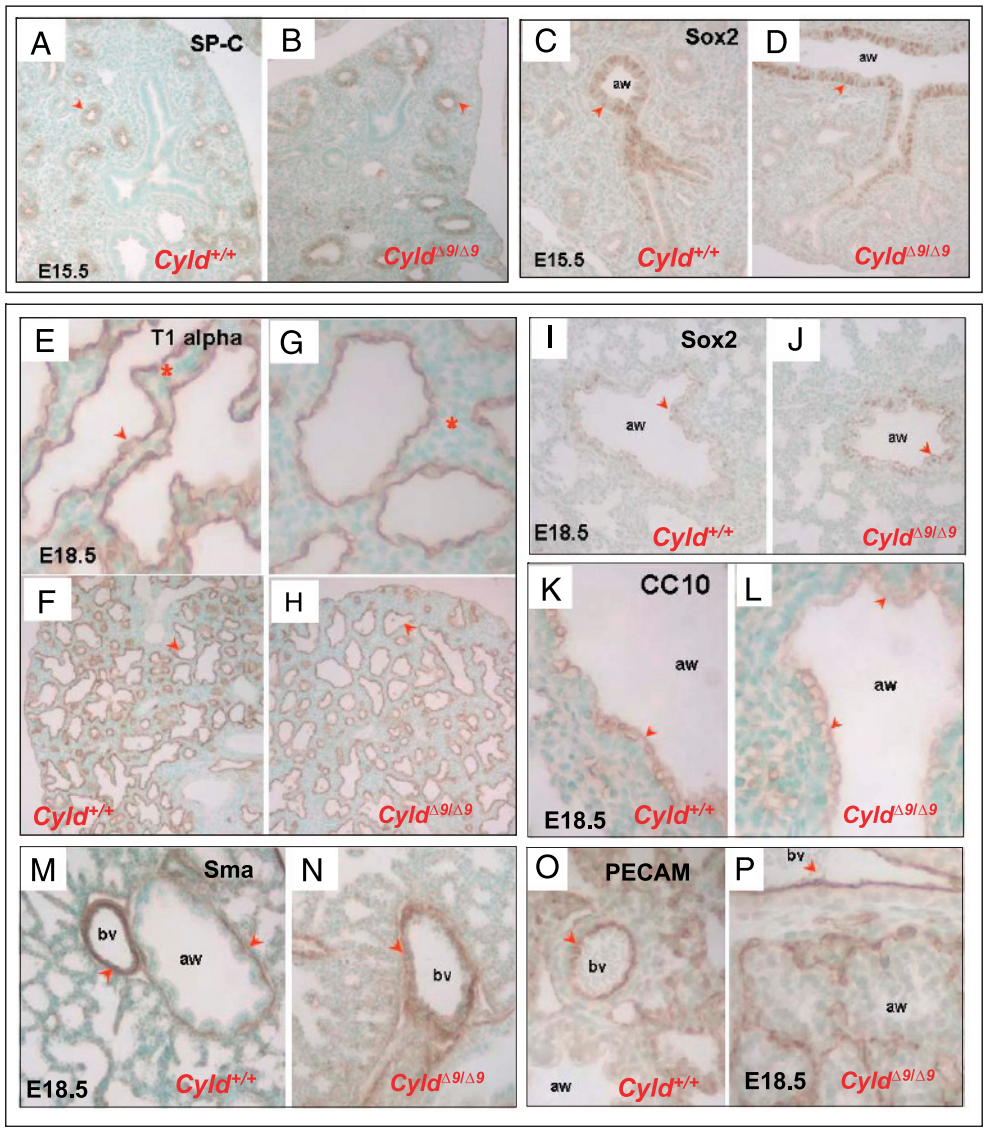

Figure 4. Immunohistochemical analysis of developing lungs from wild-type and $Cyld^{\Delta 9/\Delta 9}$ embryos. Paraffin sections of lung tissue from embryos of the indicated stage were immunostained for SP-C (A and B), CC10 (K and L), T1α (E–H), Sox2 (C, D, I, and J), Sma (M and N), and PECAM-1 (O and P). *aw* indicates airway; *bv*, blood vessel.

to exon 8. Therefore, exon 9 was flanked with loxP sites (floxed) as shown in Figure 1*A*, and the mutation was introduced to mouse embryonic stem cells through standard gene targeting procedures. Initially, we generated heterozygous $Cyld^{+/\Delta 9}$ mice by appropriate crosses between mice that carry two floxed *Cyld* alleles ($Cyld^{flx9/flx9}$) with an X-linked *cre* transgenic mouse that expresses the Cre recombinase in the germ line [22]. $Cyld^{flx9/flx9}$ and $Cyld^{+/\Delta 9}$ mice did not have any macroscopic, histological, or fertility problems. Heterozygous $Cyld^{+/\Delta 9}$ were subsequently crossed to generate homozygous $Cyld^{\Delta 9/\Delta 9}$. RT-PCR, genomic PCR, and Western blot analysis confirmed the absence of exon 9–containing *Cyld* mRNA and DNA and full-length CYLD protein in MEF from $Cyld^{\Delta 9/\Delta 9}$ embryos (Figure 1, *B–D*). However, an approximately 30-kDa polypeptide containing amino-terminal epitopes of CYLD was consistently detected in lysates from $Cyld^{\Delta 9/\Delta 9}$ MEF but not wild-type MEF lysates (Figure 1*D*). This finding is consistent with the expression of an amino-terminal fragment of CYLD, which would lack a functional deubiquitinating domain. To determine whether CYLD affects the NF-κB and JNK pathways *in vivo*, MEF from wild-type and $Cyld^{\Delta 9/\Delta 9}$ embryos were used to determine the levels of NF-κB and JNK activation in response to CD40 activation or TNF, respectively. In accordance with previous studies involving immortalized cell lines, inactivation of CYLD in our $Cyld^{\Delta 9/\Delta 9}$ mice resulted in elevated NF-κB and JNK activity (Figure 2).

$Cyld^{\Delta 9/\Delta 9}$ *Mice Die Perinatally from Apparent Respiratory Dysfunction*

$Cyld^{\Delta 9/\Delta 9}$ mice were born at normal Mendelian ratios but died shortly after birth (Table 1). Newborn $Cyld^{\Delta 9/\Delta 9}$ mice were smaller than their wild-type littermates and had short and kinky tails (15 of 15 mice examined), which may underlie a mild skeletal defect (Figure 3*A*). These mice did not show any other major external developmental defects, but their skin color suggested that they rapidly developed cyanosis. Internal examination revealed that all organs formed. However, in all newborn $Cyld^{\Delta 9/\Delta 9}$ mice examined (8/8), the lungs failed to float in the buoyancy test in isotonic solution, indicating that these mice were unable to breathe at birth (Figure 3*B*). This prompted

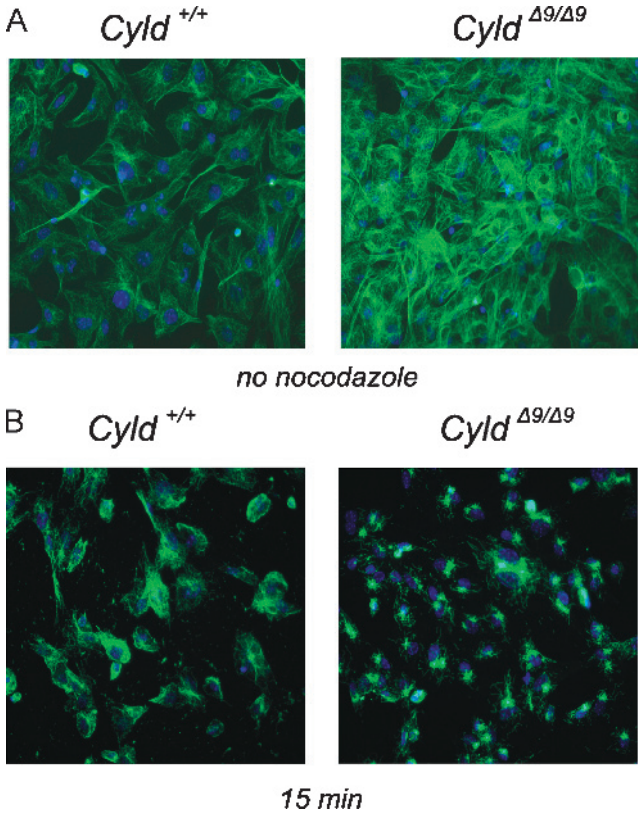

Figure 5. CYLD inactivation impairs microtubule regrowth after nocodazole treatment. Microtubules of embryonic fibroblasts from wild-type or ($Cyld^{+/+}$) or $Cyld^{\Delta 9/\Delta 9}$ embryos were visualized by immunofluorescence before nocodazole treatment (A) or 15 minutes after nocodazole washout that followed 30 minutes of treatment with nocodazole (B). A representative experiment of two independent experiments done in quadruplicates is shown.

us to characterize the phenotypic changes in these lungs and to further investigate how disruption of CYLD function interfered with lung development in $Cyld^{\Delta 9/\Delta 9}$ mice.

Abnormal Development of Lungs in $Cyld^{\Delta 9/\Delta 9}$ *Embryos*

Lungs were isolated from $Cyld^{\Delta 9/\Delta 9}$ and wild-type embryos at E13.5, E15.5, and E 18.5, representative of early and late stages of lung development, and morphological and marker analyses of these specimens were performed. Gross morphology and histological analysis (hematoxylin and eosin staining) of E13.5 and E15.5 lungs showed no abnormalities in mutants and suggested that the initial stages of lung formation and branching morphogenesis were apparently unaffected by CYLD deficiency (data not shown). However, by E18.5, mutant lungs looked slightly smaller. Hematoxylin and eosin–stained sections showed that although primitive saccules were present in the distal region of the lung, these did not seem to be expanded as in wild-type lungs. Moreover, the interstitial spaces appeared to be thicker and more densely populated by mesenchymal cells compared with wild-type littermates, suggesting overall features of lung immaturity (Figure 3*C*).

Immunohistochemical analysis showed that at E15.5 lungs from $Cyld^{\Delta 9/\Delta 9}$ and wild-type embryos have a similar pattern of expression of the distal epithelium marker SP-C and the proximal epithelium marker HMG transcription factor Sox2 (Figure 4, *A–D*). At E18.5, both wild type and mutant lungs have already undergone sacculation. By this process, distal epithelial tubules evolve into terminal saccules. This is coincident with flattening of some distal epithelial cells to form type I alveolar cells resulting in a drastic expansion of air spaces and thinning of the mesenchyme, as a preparation for birth. T1α labels type I epithelial cells, which are recognized by their flat morphology outlining the primitive saccules (reviewed in [24,25]). No difference in T1α expression was detected between wild type and mutant groups, suggesting that type I cells could differentiate in the absence of CYLD. Mutant lungs, however, showed abundant mesenchyme in between terminal saccules (compare the region depicted by asterisks in Figure 4, *E* and *G*). This is consistent with the apparent inability of these lungs to perform normal gas exchange subsequently at birth. Our results strongly suggest that immaturity in $Cyld^{\Delta 9/\Delta 9}$ lungs resulted at least in part from failure to undergo thinning of the mesenchyme. Analysis of E18.5 lungs did not reveal differences in the pattern or intensity of staining for SP-C, Sox2, CC10, Sma, or PECAM, suggesting that type II cells, Clara cells, muscular, and vascular structures were present and likely normal in $Cyld^{\Delta 9/\Delta 9}$ embryos (Figure 4, *I–P*; data not shown). Although the defect we described could already explain the lethality of $Cyld^{\Delta 9/\Delta 9}$ mice at birth, we cannot exclude central nervous system or

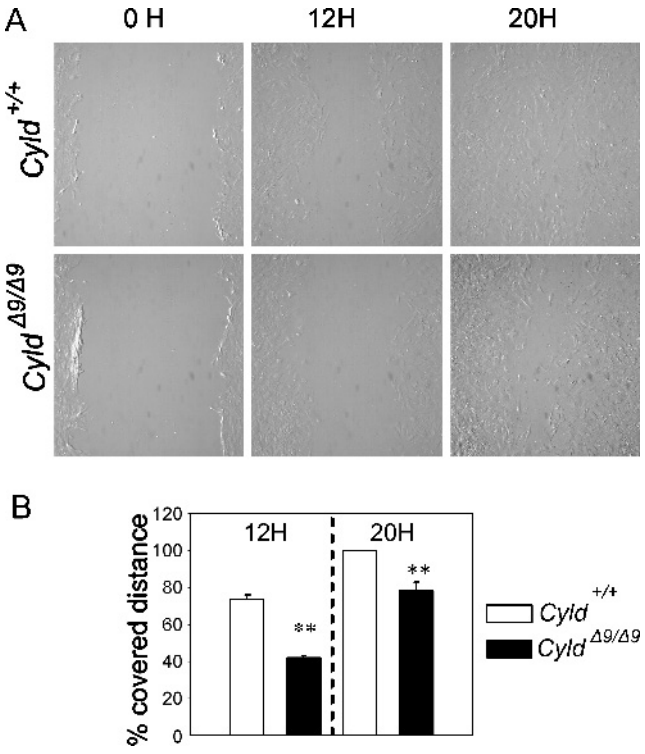

Figure 6. Wound-healing assay after nocodazole treatment. Confluent cultures of fibroblasts from wild-type or ($Cyld^{+/+}$) or $Cyld^{\Delta 9/\Delta 9}$ embryos were treated with nocodazole for 30 minutes, and after nocodazole washout, they were subjected to a standard wound-healing assay. (A) Phase-contrast images of the wound margins were acquired 12 and 20 hours after wounding. (B) The distance that was covered by migrating cells was measured at 12 and 20 hours after wounding and was expressed as percent of the initial distance that was generated by the wound. The values that are shown represent means ± SE of average distances traveled by the cells at four different segments of the wound from four experiments. Statistical analysis was performed using the Student's *t*-test. Statistically significant differences between the values that correspond to wild-type and $Cyld^{\Delta 9/\Delta 9}$ MEF are shown by ** (P value $< .01$).

neuromuscular abnormalities as contributing factors. These possibilities will be investigated in future studies.

CYLD Inactivation Impairs Microtubule Regrowth and Cell Migration After Nocodazole Treatment

CYLD has been implicated in microtubule dynamics and cell migration [26]. It is conceivable that the lung maturation defect that was observed in $Cyld^{\Delta 9/\Delta 9}$ embryos is related to the dysregulation of microtubule reorganization and cell migration associated with cellular remodeling that takes place during the late stages of embryonic lung maturation. To investigate this possibility, fibroblasts from $Cyld^{\Delta 9/\Delta 9}$ and wild-type embryos were examined for their ability to support microtubule regrowth after nocodazole treatment. Microtubule regrowth was clearly delayed in $Cyld^{\Delta 9/\Delta 9}$ MEF compared with their wild-type counterparts (Figure 5). To determine whether the delay in microtubule regrowth after nocodazole treatment can impair the migratory ability of $Cyld^{\Delta 9/\Delta 9}$ MEF, a wound healing assay was performed. For this purpose, confluent cultures of wild-type and $Cyld^{\Delta 9/\Delta 9}$ MEF were treated with nocodazole as above and then tested for their ability to fill a cell-free area that was generated by scraping the cell monolayer as described in the Materials and methods section. A significant delay in cell migration of $Cyld^{\Delta 9/\Delta 9}$ MEF compared with wild-type MEF was observed (Figure 6). There was no significant difference between the migratory ability of $Cyld^{\Delta 9/\Delta 9}$ and wild-type MEF in the absence of nocodazole pretreatment (data not shown). Furthermore, there was no significant difference in the proliferation capacity of $Cyld^{\Delta 9/\Delta 9}$ and wild-type MEF as determined by thymidine incorporation (data not shown). Taken together, these results demonstrate that inactivation of CYLD impairs postdepolymerization microtubule regrowth and associated cell migration.

Discussion

We have generated a mouse model of CYLD inactivation in all tissues, which revealed a fundamental role of functional CYLD in lung maturation. Interestingly, the respiratory dysfunction and perinatal lethality of $Cyld^{\Delta 9/\Delta 9}$ mice described in this study was not observed in other mouse models of *Cyld* inactivation that have eliminated the translation-initiation-ATG–containing exon [15,18,19], although one additional group reported perinatal lethality of mice expressing a carboxyl-terminally truncated inactive form of CYLD [27]. The reason for this apparent discrepancy might be the expression and possibly scaffolding activity of an amino-terminal catalytically inactive CYLD fragment in our mice, which would be absent from the $Cyld^{-/-}$ mice generated by Reiley et al., Massoumi et al., and Zhang et al. who targeted exon 2 or exons 2 and 3 for deletion. An alternative possibility for the difference between our $Cyld^{\Delta 9/\Delta 9}$ mice and the $Cyld^{-/-}$ mice described by Reiley et al., Massoumi et al., and Zhang et al. is that deletion of exon 2 or exons 2 and 3 allows for expression of an amino-terminally truncated and catalytically active CYLD polypeptide, the translation of which is initiated at an in-frame methionine codon downstream from exon 3.

The principal histological characteristic of lungs from E18.5 $Cyld^{\Delta 9/\Delta 9}$ embryos was an abnormally thick mesenchyme that did not allow proper formation of the alveolocapillary barrier. The enlarged mesenchymal layer of the lung could be due to impaired apoptosis and/or enhanced proliferation of mesenchymal cells or excessive epithelial to mesenchymal transition. The increased NF-κB activity that characterizes CYLD loss of function would be consistent with these possibilities [28–30]. In addition, the hyperplastic lung mesenchyme could have resulted from abnormal microtubule rearrangements and disturbed cell migration during the late stages of lung development. This possibility is supported by the role of functional CYLD in microtubule dynamics as shown by Gao et al. [26] and the present study.

The immature lung phenotype of $Cyld^{\Delta 9/\Delta 9}$ mice resembles the phenotype of mice with parathyroid hormone–related protein deficiency or enzymatic deficiencies that affect the structure of the glycosaminoglycan heparan sulfate [31–33]. Additional studies will be required to define more precisely the mechanism by which CYLD acts in maturation of the distal lung and whether CYLD exerts its effects directly in the mesenchyme or through the epithelium.

Down-regulation of CYLD has been associated with the development of lung adenocarcinomas [4]. Importantly, both embryonic lung maturation and the growth suppression of *Cyld*-deficient lung adenocarcinoma cell lines depend on the integrity of the catalytic domain of CYLD (present study and Zhong et al. [4]). It is conceivable that CYLD may regulate cellular activities and pathways in different cell layers and thus influence tumor initiation and/or progression.

Acknowledgments

The authors thank Dr. Vasso Kostourou for help with experiments described in Figures 5 and 6, Maria Alexiou and the personnel of the "Al. Fleming" animal facility for expert technical assistance, and Dr. Shao-Cong Sun (The University of Texas, MD Anderson Cancer Center) for providing the polyclonal anti-CYLD antiserum.

References

[1] Bignell GR, Warren W, Seal S, Takahashi M, Rapley E, Barfoot R, Green H, Brown C, Biggs PJ, Lakhani SR, et al. (2000). Identification of the familial cylindromatosis tumour-suppressor gene. *Nat Genet* **25**, 160–165.

[2] Massoumi R, Podda M, Fassler R, and Paus R (2006). Cylindroma as tumor of hair follicle origin. *J Invest Dermatol* **126**, 1182–1184.

[3] Hellerbrand C, Bumes E, Bataille F, Dietmaier W, Massoumi R, and Bosserhoff AK (2007). Reduced expression of CYLD in human colon and hepatocellular carcinomas. *Carcinogenesis* **28**, 21–27.

[4] Zhong S, Fields CR, Su N, Pan YX, and Robertson KD (2007). Pharmacologic inhibition of epigenetic modifications, coupled with gene expression profiling, reveals novel targets of aberrant DNA methylation and histone deacetylation in lung cancer. *Oncogene* **26**, 2621–2634.

[5] Hirai Y, Kawamata Y, Takeshima N, Furuta R, Kitagawa T, Kawaguchi T, Hasumi K, Sugai S, and Noda T (2004). Conventional and array-based comparative genomic hybridization analyses of novel cell lines harboring HPV18 from glassy cell carcinoma of the uterine cervix. *Int J Oncol* **24**, 977–986.

[6] Costello CM, Mah N, Hasler R, Rosenstiel P, Waetzig GH, Hahn A, Lu T, Gurbuz Y, Nikolaus S, Albrecht M, et al. (2005). Dissection of the inflammatory bowel disease transcriptome using genome-wide cDNA microarrays. *PLoS Med* **2**, e199.

[7] Annunziata CM, Davis RE, Demchenko Y, Bellamy W, Gabrea A, Zhan F, Lenz G, Hanamura I, Wright G, Xiao W, et al. (2007). Frequent engagement of the classical and alternative NF-kappaB pathways by diverse genetic abnormalities in multiple myeloma. *Cancer Cell* **12**, 115–130.

[8] Jenner MW, Leone PE, Walker BA, Ross FM, Johnson DC, Gonzalez D, Chiecchio L, Dachs Cabanas E, Dagrada GP, Nightingale M, et al. (2007). Gene mapping and expression analysis of 16q loss of heterozygosity identifies WWOX and CYLD as being important in determining clinical outcome in multiple myeloma. *Blood* **110**, 3291–3300.

[9] Keats JJ, Fonseca R, Chesi M, Schop R, Baker A, Chng WJ, Van Wier S, Tiedemann R, Shi CX, Sebag M, et al. (2007). Promiscuous mutations activate the noncanonical NF-kappaB pathway in multiple myeloma. *Cancer Cell* **12**, 131–144.

[10] Massoumi R and Paus R (2007). Cylindromatosis and the *CYLD* gene: new lessons on the molecular principles of epithelial growth control. *Bioessays* **29**, 1203–1214.
[11] Kovalenko A, Chable-Bessia C, Cantarella G, Israel A, Wallach D, and Courtois G (2003). The tumour suppressor *CYLD* negatively regulates NF-kappaB signalling by deubiquitination. *Nature* **424**, 801–805.
[12] Trompouki E, Hatzivassiliou E, Tsichritzis T, Farmer H, Ashworth A, and Mosialos G (2003). CYLD is a deubiquitinating enzyme that negatively regulates NF-kappaB activation by TNFR family members. *Nature* **424**, 793–796.
[13] Reiley W, Zhang M, and Sun SC (2004). Negative regulation of JNK signaling by the tumor suppressor *CYLD*. *J Biol Chem* **279**, 55161–55167.
[14] Yoshida H, Jono H, Kai H, and Li JD (2005). The tumor suppressor cylindromatosis (*CYLD*) acts as a negative regulator for toll-like receptor 2 signaling via negative cross-talk with TRAF6 and TRAF7. *J Biol Chem* **280**, 41111–41121.
[15] Reiley WW, Zhang M, Jin W, Losiewicz M, Donohue KB, Norbury CC, and Sun SC (2006). Regulation of T cell development by the deubiquitinating enzyme CYLD. *Nat Immunol* **7**, 411–417.
[16] Reiley WW, Jin W, Lee AJ, Wright A, Wu X, Tewalt EF, Leonard TO, Norbury CC, Fitzpatrick L, Zhang M, et al. (2007). Deubiquitinating enzyme CYLD negatively regulates the ubiquitin-dependent kinase Tak1 and prevents abnormal T cell responses. *J Exp Med* **204**, 1475–1485.
[17] Jin W, Reiley WR, Lee AJ, Wright A, Wu X, Zhang M, and Sun SC (2007). Deubiquitinating enzyme CYLD regulates the peripheral development and naive phenotype maintenance of B cells. *J Biol Chem* **282**, 15884–15893.
[18] Massoumi R, Chmielarska K, Hennecke K, Pfeifer A, and Fassler R (2006). Cyld inhibits tumor cell proliferation by blocking Bcl-3–dependent NF-kappaB signaling. *Cell* **125**, 665–677.
[19] Zhang J, Stirling B, Temmerman ST, Ma CA, Fuss IJ, Derry JM, and Jain A (2006). Impaired regulation of NF-kappaB and increased susceptibility to colitis-associated tumorigenesis in CYLD-deficient mice. *J Clin Invest* **116**, 3042–3049.
[20] Hovelmeyer N, Wunderlich FT, Massoumi R, Jakobsen CG, Song J, Worns MA, Merkwirth C, Kovalenko A, Aumailley M, Strand D, et al. (2007). Regulation of B cell homeostasis and activation by the tumor suppressor gene *CYLD*. *J Exp Med* **204**, 2615–2627.
[21] Douni E, Alexiou M, and Kollias G (2004). Genetic engineering in the mouse: tuning TNF/TNFR expression. *Methods Mol Med* **98**, 137–170.
[22] Schwenk F, Baron U, and Rajewsky K (1995). A *cre*-transgenic mouse strain for the ubiquitous deletion of loxP-flanked gene segments including deletion in germ cells. *Nucleic Acids Res* **23**, 5080–5081.
[23] Hatzivassiliou E, Miller WE, Raab-Traub N, Kieff E, and Mosialos G (1998). A fusion of the EBV latent membrane protein-1 (LMP1) transmembrane domains to the CD40 cytoplasmic domain is similar to LMP1 in constitutive activation of epidermal growth factor receptor expression, nuclear factor-kappa B, and stress-activated protein kinase. *J Immunol* **160**, 1116–1121.
[24] Cardoso WV and Lu J (2006). Regulation of early lung morphogenesis: questions, facts and controversies. *Development* **133**, 1611–1624.
[25] Williams MC (2003). Alveolar type I cells: molecular phenotype and development. *Annu Rev Physiol* **65**, 669–695.
[26] Gao J, Huo L, Sun X, Liu M, Li D, Dong JT, and Zhou J (2008). The tumor suppressor *CYLD* regulates microtubule dynamics and plays a role in cell migration. *J Biol Chem* **283**, 8802–8809.
[27] Ermolaeva M, Sebban H, Courtois G, and Pasaparakis M. Early postnatal lethality in knock-in mice expressing a truncated catalytically inactive form of CYLD. In: NF-kappaB: 20 Years on the Road from Biochemistry to Pathology, Keystone Symposia; March 23–28, 2006; Fairmont Banff Springs, Banff, Alberta, Canada.
[28] Fan Y, Dutta J, Gupta N, Fan G, and Gelinas C (2008). Regulation of programmed cell death by NF-kappaB and its role in tumorigenesis and therapy. *Adv Exp Med Biol* **615**, 223–250.
[29] Van Waes C (2007). Nuclear factor-kappaB in development, prevention, and therapy of cancer. *Clin Cancer Res* **13**, 1076–1082.
[30] Min C, Eddy SF, Sherr DH, and Sonenshein GE (2008). NF-kappaB and epithelial to mesenchymal transition of cancer. *J Cell Biochem* **104**, 733–744.
[31] Rubin LP, Kovacs CS, De Paepe ME, Tsai SW, Torday JS, and Kronenberg HM (2004). Arrested pulmonary alveolar cytodifferentiation and defective surfactant synthesis in mice missing the gene for parathyroid hormone–related protein. *Dev Dyn* **230**, 278–289.
[32] Li JP, Gong F, Hagner-McWhirter A, Forsberg E, Abrink M, Kisilevsky R, Zhang X, and Lindahl U (2003). Targeted disruption of a murine glucuronyl C_5-epimerase gene results in heparan sulfate lacking L-iduronic acid and in neonatal lethality. *J Biol Chem* **278**, 28363–28366.
[33] Fan G, Xiao L, Cheng L, Wang X, Sun B, and Hu G (2000). Targeted disruption of *NDST-1* gene leads to pulmonary hypoplasia and neonatal respiratory distress in mice. *FEBS Lett* **467**, 7–11.